Non-Relativistic Anisotropic Magnetoresistance

P. Ritzinger,[1] few others,[1] and K. Výborný[1]

[1] *Institute of Physics, ASCR, v. v. i., Cukrovarnická 10, CZ-16253 Praha 6, Czech Republic*

(Dated: Mar17, 2025)

Anisotropic magnetoresistance (AMR) is usually attributed to interplay of magnetic order with spin-orbit interaction. We show that the latter is not necessary using two examples: one with collinear magnetic order (where however, the anisotropy is likely to remain fixed) and another example with non-collinear order where magnetic moments can be manipulated by magnetic field.

I. INTRODUCTION

Discovered by William Thomson in 1857,[1] as the resistance in ferromagnetic cobalt and nickel being dependent on the direction of the magnetization, the AMR has been subject of research ever since.[2] In a still widespread belief, AMR is often described as an effect, which occurs in ferromagnets and has a two-fold (or 180°-periodic) dependence on the angle ϕ between current and magnetization[3], thus:

$$\frac{\Delta\rho}{\rho} \propto \cos 2\phi \tag{1}$$

In transition metals, this effect is attributed to the scattering of delocalized s-electrons into localized d-states at magnetic impurities through spin-orbit coupling (SOC)[4]. In this work, we are going to explain how AMR can be realized in the absence of SOC either 'by itself' or due to non-collinear magnetic order, rendering it a non-relativistic effect.

A. Overview on Anisotropic Magnetoresistance

Before we turn towards the realization of non-relativistic AMR, we will have a look on current developments of AMR, since many aspects of that simplistic view on AMR have been already corrected: AMR has been reported in other magnetically ordered materials, such as the antiferromagnetic MnTe[5,6] and CuMnAs[7–9], and ferrimagnetic Mn_4N[10]. Higher-order symmetries in the AMR signal have been reported, such as four-fold signals in nickel[11], Co_2MnGa[13,14] or (Ga, Mn)As[15,16], six-fold signals in hexagonal MnTe[5,6] and sometimes even higher symmetries[6,17]. Furthermore, AMR has even been reported when the magnetization rotated perpendicular to the current direction[13,15,18]. The latter two effects occur in good crystalline quality and are referred to as *crystalline AMR*[13,16], while the merely two-fold signal which prevails in polycrystalls is called *non-crystalline AMR*. Although this is known for almost a century[11], it is often times confused with magnetocrystalline anisotropy[2] or some people refer to it as a newly discovered effect[19].

Another possible classification of AMR is extrinsic and intrinsic AMR. The former is the classical scattering-dependent AMR and has been the center of attention for a long time. The intrinsic AMR has only came to attention recently[20,21] and is scattering-independent. Only a few studies acknowledge scattering-independent contributions to the AMR[45–48]. It was shown experimentally that it is possible to distinguish extrinsic and intrinsic AMR by means of frequency-dependent AMR[20,21]: The extrinsic contribution scales roughly with $1/\omega$, while the intrinsic contribution is frequency-independent[20]. Intrinsic effects spurred a larger interest in other branches of spintronics, for example the intrinsic Anomalous Hall effect (AHE) or spin Hall effect (SHE). In these effects the intrinsic component is usually linked to the Berry curvature[42,43], which is different from the AMR, which can be related to the topology of the Fermi surface as will be elaborated in Sec. III.

This shall only serve as a short introduction to the topic of Anisotropic Magnetoresistance. A more comprehensive overview can be found in Ref.[2]

B. Non-collinear Magnetic Order

All of these previous considerations still necessitate and assume the existence of spin-orbit coupling. Recently, it has been shown that other features such as spin textures[22] and spin torque[23] can be realized by means of non-collinear magnetic order under neglectance of SOC. This means, that non-collinar magnetic order can mimick some properties of SOC and can thus render these effects non-relativistic.

The non-collinear antiferromagnet Mn_3Sn recently experiences increased attention due to its unique properties: It is considered to be a Weyl semimetal with chiral anomaly[31–34,38,40,41] and shows large Anomalous Hall effect (AHE)[31–33,36,39] as well as Anomalous Nernst effect (ANE)[31,32,36,37] and spin Hall effect (SHE)[36,42]. For AHE and SHE strong intrinsic were found[42]. A local (sublattice-projected) Edelstein effect was found in this material[23].These effects prevail even in the absence of spin-orbit coupling (SOC) due to its non-collinear magnetic order[23,32]. Mn_3Sn has considerable potential for future spintronic devices[31–33] due to spin-polarized charge currents[39], ultrafast spin dynamics[31,33]. Reading and writing of domains was shown by laser heating and ANE measurements, respectively[41].

Mn_3Sn has a hexagonal Ni_3Sn[33] type structure. Below its Néel temperature of approx $420 - 430$ K[31,33–37] it has

a triangular non-collinear order of magnetic moments, we will consider in this work. For lower temperatures, transitions of the magnetic order to a helical phase and finally a spin glass phase are reported[31,34,38], and seem to depedend on the stoichiometry[38], which, however, goes beyond the scope of this work. Due to its similarity, the components are often summarized into Mn_3X[31] where X is typically Ge[31,32,34,35,40] or Ir[23,39].

Experimental results of AMR and its transversal counterpart (often referred to as planar Hall effect, or PHE) in Mn_3Sn and Mn_3Ge have been reported: The AMR is usually two-fold[31,34,40], while in one study a four-fold signal was reported at $T = 10$ K, which vanished at higher temperatrues and was attributed to tilting Weyl nodes[40]. Temperature and field dependence were investigated briefly as well: The PHE was reported to be higher at 100 K than at 300 K[31] and the AMR increased upon increasing applied magnetic field[34]. In the helical phase, no AMR was reported, where in the spinglass phase the AMR was also two-fold[34]. The problem about the definition is discussed in the next section. The results might appear to be less conclusive than in simpler FM or collinear AFM systems due to the rather involved non-collinear magnetic order, which will be discussed at the end of Sec. II in more detail.

Its a kagome lattice (ref to Edelstein and Hyami?) ...

The comparably lesser known CrSe exhibits a NiAs-type structure[26]. Its non-coplanar antiferromagnetic order prevails below its Néel temperature of $T_N = 280K$[27,28]. It shows a double-layer triangular structure, where within each layer, the moments in the xy-plane are cancelling each other out, while there is finite z-moment. The magnetic moments of the second layer are exactly the opposite of the first layer. The CrSe compounds belong to the family of Cr_nX (X = S, Se, Te, and Sb), which, again show very different properties based on n and X[27,28]. However, Cr_nX for $n \neq 1$ and $X \neq$ Se is beyond the scope of this work. CrSe appears to be sensitive to off-stoichiometry, thickness or growth temperature, where, for instance, a semiconductor-to-metal transition was induced by varying the growth temperature[28]. CrSe grown on the topological insulator $(Bi, Sb)_2Te_3$ showed ferromagnetism as a result of proximity effects[29].

C. Organization

In this paper we will show how AMR can be achieved by non-collinear magnetic order while neglecting SOC and thus, rendering AMR an non-relativistic effect. We are modelling the various non-collinear systems using a tight-binding model. We will realize non-relativistic AMR in two different ways: Intrinsically, thus scattering-independent, due to an anisotropic Fermi surface and extrinsically by considering magnetic impurities.

In both cases, we will start by considering non-collinear magnetic order on a kagome lattice (see Fig. 1) and a triangular lattice (see Fig. 2). Both lattices are all based on a triangular lattice. In case of the kagome lattice, regular vacancies (which in practice can be filled by non-magnetic atoms) are creating a structure consisting of triangles and hexagons. In case of the intrinsic AMR, we are concluding shortly by considering real materials whose structure we got from MAGNDATA data base: CrSe[53] and Mn_3Sn[52]. For the extrinsic AMR, one other toymodels is introduced: A square lattice with ferromagnetic moments, where the magnetic moments point along $\hat{y}$.

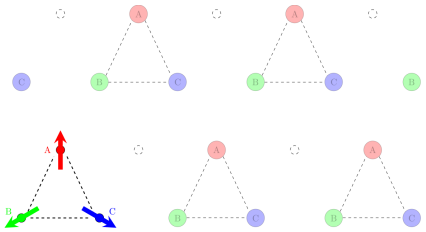

FIG. 1. Schematic image of the kagome lattice with non-collinear magnetic order. The three magnetic moments in the magnetic unit cell are shown in red, green and blue. The net magnetic moment is zero. While the magnetic unit cell is the same as in the triangular lattice, the regular vacancy distinguishes the two. In practice, the vacancy can be filled with a non-magnetic atom.

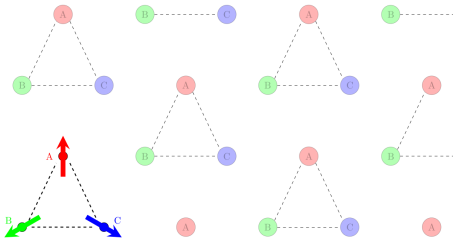

FIG. 2. Schematic image of the triangular lattice with non-collinear magnetic order. The three magnetic moments in the magnetic unit cell are shown in red, green and blue. The net magnetic moment is zero.

This paper is organized as follows: In Sec. II, we will introduce the model. In Sec. III, we will discuss intrinsic AMR (both for collinear MnN and for non-collinear AFMs), followed by the discussion of extrinsic AMR in non-collinear AFMs (Sec. IV). What about ab initio

II. MODELLING

A. Formalism

We employ a simplistic tight-binding model which only consists of a hopping and an exchange term[23]:

$$H = -\sum_{i,j}\sum_{\alpha} t_{ij}\hat{c}_i^{\alpha\dagger}\hat{c}_j^{\alpha} + J\sum_i\sum_{\alpha,\beta}(\vec{\sigma}\cdot\hat{m}_i)_{\alpha\beta}\hat{c}_i^{\alpha\dagger}\hat{c}_i^{\beta} \quad (2)$$

where t_{ij} is the hopping parameter from site i to j, α and β are the spin indices, $\hat{c}_i^{\alpha}(^{\dagger})$ is an annihilation (creation) operator at site i with spin α, J is the Heisenberg exchange constant, $\vec{\sigma}$ the vector of the Pauli spin matrices and $\hat{m}_i$ the magnetization direction unit vector at site i.

The conductivity is then calculated using the Boltzmann equation[25].

$$\sigma_{ij} = e^2 \sum_n \int_{1stBZ} \frac{d^3k}{(2\pi)^3} \delta(E_n(\vec{k}) - E_F) \frac{1}{\hbar \Gamma_{n,\vec{k}}} \times v_{n,i}(\vec{k}) v_{n,j}(\vec{k}) \quad (3)$$

where e is the elementary charge, $E_n(\vec{k})$ is the k-dependent Eigen energy of the nth-band, E_F is the Fermi energy, $\Gamma_{n,\vec{k}}$ is the scattering rate and $v_{n,i}$ is the i-th component of the Fermi velocity in the n-th band. The delta distribution evaluates the integral over the first Brillouin zone (1st BZ) at the Fermi surface. The Fermi velocity is calculated by:

$$v_{n,i} = \frac{1}{\hbar} \frac{\partial E_n(\vec{k})}{\partial k_i} \quad (4)$$

The scattering rate is obtained by using Fermi's Golden Rule:

$$\Gamma_{n,\vec{k}} = \frac{2\pi}{\hbar} N_{scat} \sum_{n'} \int_{1stBZ} \frac{d^3k'}{(2\pi)^3} \delta(E_{n'}(\vec{k'}) - E_n(\vec{k})) \times |M_{nn'}^{\vec{k}\vec{k'}}|^2 (1 - \cos\theta_{vv'}) \quad (5)$$

where N_{scat} is the volume density of the scatterers, $M_{nn'}^{\vec{k}\vec{k'}}$ is the transition matrix element and $\cos\theta_{vv'} = \frac{\vec{v}_n(\vec{k})}{|\vec{v}_n(\vec{k})|} \frac{\vec{v}'_n(\vec{k'})}{|\vec{v}'_n(\vec{k'})|}$. The transition matrix element is calculated by:

$$M_{nn'}^{\vec{k}\vec{k'}} = \langle \psi_{n,\vec{k}} | \hat{M} | \psi_{n',\vec{k'}} \rangle \quad (6)$$

where $\psi_{n,\vec{k}}$ is the wave function for the Eigenenergy value $E_n(\vec{k})$[25].

B. Definition of AMR

The anisotropy of resistance can be expressed as a percentage in the AMR ratio, thus $\Delta\rho/\rho \neq 0$[2] or by equivalently looking at the respective conductivities. There is two different ways, how this can be defined: Either we keep the magnetic order constant and then look at the conductivities at two different directions, e.g. $\sigma_{xx}/\sigma_{yy} \neq 1$ or we keep the direction of measurement constant, but rotate the magnetic order, e.g. $\sigma_{xx}(\vec{M}_{\perp})/\sigma_{xx}(\vec{M}_{\parallel}) \neq 1$. Using the first configuration with the static magnetic order is usually more unhandy in experiment, but allows us to define the AMR as a spontaneous effect[44]. Utilizng this definition, we can understand that forms of non-relativistic AMR deviating from our definition exist, which can be illustrated at the example of the antiferromagnetic MnN, which consists of FM layers aligned antiparallel to each other[51].

Another example of non-relativistic AMR can be found in antiferromagnetic $EuTe_2$. The material undergoes a metal-insulator transition (MIT), where the critical field and temperature is different in the ab-plane than it is along the c-axis. Measuring σ_{xx} while rotating the magnetic field can then cause AMR of up to 40000% due to the insuing MIT[54]. Both of the latter examples, MnN and $EuTe_2$ are different mechanisms for non-relativistic AMR than in our approach utilizing non-collinear magnetic order.

Apart from AMR ratios, it is also possible to track angle-dependent MR which in its simplest form is shown in Eq. 1. In FMs and collinear antiferromagnets, a single spin axis (SSA) exists, which is the magnetization and the Néel vector, respectively. It is assumed, that an applied magnetic field serves to rotate the SSA, which in turn creates the AMR signal. In non-collinear systems, no such SSA exist (that is, even if the applied magnetic field creates a small magnetization, the underlying magnetic order is still much more involved than in FMs). Interpretations of how AMR works are thus diverging: In Ref. 40 it is, for example, assumed that all spins are rotated at the same time by the magnetic field, ignoring possible tilts. Rotating all spins at the same time would not lead to any results in our case, since in absence of the SOC, the spin is not coupled to the lattice[23]. Also, AMR is due to the magnetic order and not due to orbital effects[2], which is usually ensured by comparing measurements of longitudinal and transversal magnetoresistance (LMR and TMR, respectively)[44] or by assuming that saturation has been reached[13]. In non-collinear systems this can be more difficult as can be seen in the LMR and TMR measurements in Mn_3Sn in Fig. 5f of Ref. 31, where the expected parallel course of LMR and TMR is not reached within the field range of up to roughly 10 T.

For the intrinsic AMR, we will rotate the magnetic moments individually, as a rotation of all moments simulatenously would not produce any effect due to missing SOC. This individual rotation can be justified by assuming that the magnetic field would be large enough to partially overcome the exchange interaction. For the extrinsic AMR, the moments are kept in their original position and we are either comparing σ_{xx} with σ_{yy}, thus making use of the spontaneous effect definition; or we are only rotating the magnetic impurity while keeping all other moments at their position assuming that the impurity bound much less by exchange interaction than the regular moments.

C. An Expanded Phenomenological Model

The angle-dependent form of AMR can be expressed phenomenologically in terms of power expansion of the magnetization direction[11,15,16] and allows to describe even more complex crystalline AMR signals[6,13,17]. However, these models rely on the existence of a SSA as the magnetization or Néel vector. In non-collinear systems such SSA does not exist - even in case of weak ferromagnetism induced by an applied magnetic field, it would be likely an oversimplification to ignore the effects of the sublattices (find paper about weak ferromagnetism in Mn3Sn doesnt play a role ... sth from Jakub I think). "Local" treatment of effects is not new: For instance, basic AMR models in FMs rely on seperate contributions for spin up and spin down electrons (two-current models)[2], or the Edelstein effect in non-collinear Mn_3Sn can be calculated for each sublattice[23]. Such local approach can be applied to AMR by considering the contributions of each magnetic sublattice (MSL) individually in the phenomenological model, which yields:

$$\rho_{yy} = \rho_0 + \sum_{m=1,2,3} \sum_{n=2,4,6,\dots} c_{m,n} \cos(n\alpha_m) \tag{7}$$

where m is the index of the MSL, n is the order of the spherical harmonic, $c_{m,n}$ is the index of the n-th harmonic of the m-th MSL, and α_m is the angle of the magnetization direction of the m-th magnetic moment (assuming an in-plane rotation). The coefficients $c_{m,n}$ can be obtained by fitting where for multiple MSLs measurements for different values of magnetic field B are necessary. The position of the magnetic moments α_m can be obtained from SW models. While this is not going to be a main focus of this work, Eq. 7 together with an adequate SW model could help to distinguish the MCA from the AMR.

III. INTRINSIC AMR

As mentioned previously, intrinsic AMR means that the anisotropy of the resistivity (or conductivity) $\sigma_{xx}/\sigma_{yy} \neq 1$ (or simply $\sigma_{xx} \neq \sigma_{yy}$) is of scattering-independent origin. For now, we will exclude the option of scattering-dependent anisotropy by choosing the relaxation time approximation (RTA)[12] and replace Eq. 5 by:

$$\tau = \frac{1}{\hbar \Gamma_{n,\vec{k}}} \tag{8}$$

where the relaxation time τ is constant and thus isotropic. This means that the anisotropy can only enter through the Fermi velocity contribution (or anisotropic plasma frequencies ω^p). We can simplify Eq. 3 to:

$$\sigma_{ii} \propto \int_{FS} \sum_n dk_F v^2_{n,i}(\vec{k_F}) \tag{9}$$

where $\vec{k_F}$ is the wave vector at the Fermi surface (Fermi vector). We made use of the facts that we only consider the longitudinal conductivity σ_{ii} in two dimensional systems, the delta distribution evaluates the integral over the first Brillouin zone at the Fermi surface (FS), and the scattering rate is obtained by RTA. $\sigma_{xx} \neq \sigma_{yy}$ if the integral of $\sum_n v^2_{n,x}$ and $\sum_n v^2_{n,y}$ over the Fermi circle are not the same. This is generally achieved by anisotropic Fermi surfaces, whereas the FS must neither be spherical (which is perfect isotropic) nor show the symmetry of the system, since the conductivity must reflect the crystal symmetry due to Neumann's principle[13] (e.g. a hexagonal FS in a hexagonal material is insufficient). The results are summarized in the following subsections, starting with the cubic collinear AFM MnN and then proceeding to kagome lattice.

A. Anisotropy due to magnetic order in collinear systems

As discussed by Granville et al.[24] MnN is a cubic (rocksalt) crystal which, were it not for magnetic order, would have $\sigma_{xx} = \sigma_{yy} = \sigma_{zz}$. The cation (manganese) magnetic moments, however, prefer an A-type AFM order and in choosing the direction of the ferromagnetic planes (e.g. xy-planes), anisotropy arises (in that case, σ_{zz} is different from $\sigma_{xx} = \sigma_{yy}$). This effect in itself is non-relativistic in nature. Calculations based on density functional theory (DFT as detailed in Appendix A), show that $\hbar\omega^p_{xx} = 5.87$ eV and $\hbar\omega^p_{zz} = 5.23$ eV so that, assuming isotropic scattering, $\sigma_{xx}/\sigma_{zz} - 1 \approx 26$ %

Magnetic order leads to distortion of lattice but this effect has only minor influence on such transport anisotropy...

B. Kagome lattice

Turning to non-collinear systems, we first start by considering magnetic configurations, which are not changing the principle properties of the system, meaning that all moments will remain in the xy-plane and the moments cancel out (hence the system is perfectly compensated). Starting from the original configuration of moments as shown in Fig. 1, there are two possibilities: First, by permutations, which one is shown in Fig. 3, and second, by rotating all moments at the simultaneously. In both cases, regardless the permutation or angle of rotation, intrinsic AMR cannot be found and furthermore the results are equivalent (as well in band structure and Fermi surface) to the results shown in Fig. 3. This is, as mentioned prior, because due to the lack of SOC, spin and lattice are decoupled[23]. Nevertheless, as shown in Fig. 3 (d) and (f) to be attached, the spintexture changes depending on the permutation.

In the next step, we are individually rotating the magnetic moments within the xy-plane as shown in Figs. 8

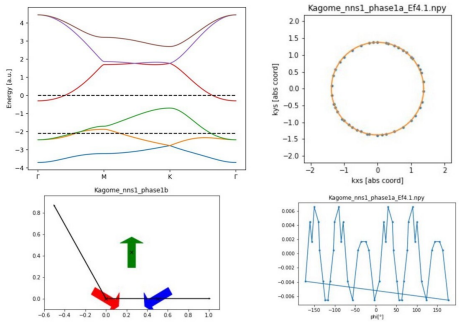

FIG. 3. Results for the kagome lattice, where the moments are permuted as compared to Fig. 1 (left lower panel). Left upper panel: The Bandstructure is spin-split. Right upper panel: The Fermi surface (Ef, band?) is represented by the blue dots. The orange circle is shown for illustration. Since the FS and the circle overlap, this system has an isotropic FS and does not show intrinsic AMR. Right lower panel: Difference of the FS points the circle. The FS is thus not perfectly spherical, but shows some six-fold modulation, which still does not allow for intrinsic AMR since in a hexagonal system, this corresponds to a symmetry operation.

and 9 (Figs to be replaced). In both cases, the unequal rotation of the moments causes a small in-plane magnetization to emerge.

- Describe the rotation of red and blue moment. we are passing some special cases: ferrimagnetism (60), permutation (120), ferromagnetism (240).
- Name, that there is always AMR, except compensated or FM state
- Now, change the moment that is "fix" and rotate again: The FS will be rotated (include example from 36 deg) → propose an experiment (since the "fixing the other moment" refers to changing the direction of applied magnetic field)
- Curiosity: In the ferrimagnetic order, despite being collinear, the FS is still two-fold and intrinsic AMR is produced. Furthermore, the FS can not only be rotated by "fixing" the other moment, but also by permutation

Hold on: What IF the in-plane magnetization is actually the cause of the AMR? See AMR in FM: as in Eq. 1 where α is the angle of rotation of magnetization. What if here: the small emerging magnetization is indeed the order parameter and the ncoll order is replacing simply the SOC?

C. Triangular lattice

In case of the triangular lattice, the same operations were applied as for the kagome lattice. In both the compensated states (simultanous rotation, and the permutation of moments) and the non-compensated states show no anisotropic Fermi surface and hence, intrinsic AMR could not be found in this system. We attribute this to a higher symmetry the system shows which one? And what more?

D. CrSe and Mn_3Sn

Now we are moving towards the real materials CrSe and Mn_3Sn. CrSe has a double layer triangular lattice, where the in-plane magnetic moments within each plane cancel out. The magnetic moments have an out-of-plane component, which gives every individual plane an out-of-plane moment, which is canceled out in the entire system since the out-of-plane component of the second plane is oriented antiparallely. The three-dimensionality of the components render CrSe non-coplanar. Contrary to the toy models, we need to take into account more next neighbors to get realistic results: Calculations with CrSe where all moments are FM serve as sanity check and need to be isotropic, which for ten next neighbors is the case. In the case of CrSe, neither the antiferromagnetic non-coplanar shows an anisotropic FS and intrinsic AMR, nor a non-compensated rotation similar to the case of kagome (describe, and describe in kagome the 36 deg more).

Secondly, we investigated Mn_3Sn, which has a double layer kagome lattice. The in-plane magnetic moments within each plane cancel out. There is no out-of-plane component of the magnetic moment, which makes it a coplanar, non-collinear magnetic. In case of Mn_3Sn, we need to take into account 20 next neighbors to get a realistic result for the FM. In the compensated case, we again do not get an anisotropic FS and thus no AMR, but in the non-compensated case, we can achieve intrinsic AMR. Thus, this system behaves similar to the kagome toy model.

Add an image: non-compensated Mn3Sn configuration, FS, FS polar plot

CrSe has nns = 10 (10 next neighbors), Mn3Sn has nns = 20 taken into account, kagome and triangular only nns = 1.

IV. EXTRINSIC AMR

Now, we are going to move towards the extrinsic AMR. In this section we will revert to the full treatment of scattering via Eq. 5. We will assume magnetic impurities pointing in $\vec{i}$-direction described by the transition matrix matrix $\hat{M} = \hat{S}_i \otimes \hat{1}_{NxN}$, where $\hat{S}_i$ is the i-th Pauli spin matrix and $\hat{1}_{NxN}$ is the N-dimensional identity matrix. For simplicity reasons, we will restrict ourselves to impurities either pointing along $\hat{x}$, as illustrated in Fig. 4, which shall be abbreviated as $\hat{x}$-impurities henceforth, and impurities along $\hat{y}$, denoted as $\hat{y}$-impurities.

Here, we are choosing three types of setups: A kagome lattice, a triangular lattice, and as reference a square

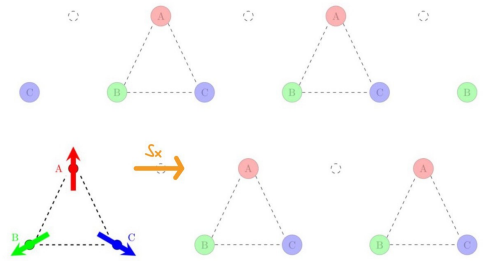

FIG. 4. Illustration of a x-impurity in a kagome lattice

Lattice	Impurity $\hat{M}$	AMR?	Spintexture
Kagome	**X**	**Yes**	XY
Kagome	**Y**	**Yes**	XY
Kagome (non-comp.)	**X**	**Yes**	XY
Kagome (non-comp.)	**Y**	**Yes**	XY
Triangular	X	divergent	Z
Triangular	Y	divergent	Z
Triangular (non-comp.)	X	No	ZY
Triangular (non-comp.)	Y	No	ZY
Square FM	X	divergent	Y
Square FM	Y	No	Y

TABLE I. Results of the extrinsic AMR calculations for the various types of lattices and impurities as introduced in the text. "Yes" means that AMR was found, hence $\sigma_{xx} \neq \sigma_{yy}$ while for "No" an isotropic behavior was identified, where $\sigma_{xx} = \sigma_{yy}$. The value of the AMR ratio is not stated here, as our model is qualitative and quantitative values would not have any real meaning. Divergent means that both σ_{xx} and σ_{yy} are divergent or infinite and AMR cannot be defined, originating from a suppressed scattering rate $\Gamma \to 0$. The spintexture...

lattice with a ferromagnetic order in $\hat{y}$-direction. We then calculate the conductivities σ_{xx} and σ_{yy} using the Eqs. 3-6. The results are summarized in table I.

In the kagome case, for both the $\hat{x}$- and the $\hat{y}$-impurity in both the compensated and non-compensated case, non-zero AMR can be found. In the triangular case, no AMR has been identified at all. In case of the square FM lattice, no AMR was found at all. In some cases the results in Tab. I are denoted by *divergent*, which means that both σ_{xx} and σ_{yy} are divergent or infinite. This originates from a suppressed scattering due to that impurity $\Gamma \to 0$ and the fact that the inverse scattering rate is part of the Boltzmann equation Eq. 3. Since our model is very simplistic, it is, however, not expected that in a real system the conductivity would diverge.

The momentum-space spintextures of the kagome lattice and the square FM are shown in Fig. 5. Spin textures can be an important tool as already shown in the context of the non-relativistic Edelstein effect[23]. Spin texture ref's: 14, 29, 34 for ncoll and 20-31 for coll in[23]. In our case, it can give us a hint about the possibility of AMR due to its similiarty: The i-th component of the

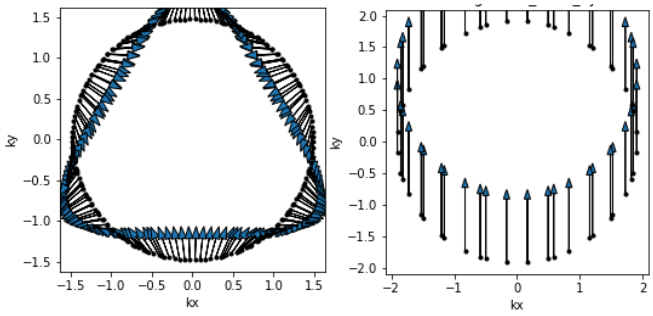

FIG. 5. The spintexture of the kagome (left) and square FM (right) lattice. In case of the square FM, all spins point in $+\hat{y}$-direction. The $\hat{z}$-component (not shown) is zero in both cases.

spin texture is given by:

$$S_i(\vec{k}) = \langle \psi_k | \hat{S}_i | \psi_k \rangle \tag{10}$$

where ψ_k is the wave function at $\vec{k}$. The scattering rate Γ at the same $\vec{k}$ for a magnetic impurity in direction i described by $\hat{S}_i$:

$$\Gamma_{\vec{k}} \propto \int_{FS} dk' |\langle \psi_k | \hat{S}_i | \psi_k \rangle|^2 \tag{11}$$

where in Eq. 11 we ignored $\cos\theta_{vv'}$ and the prefactors, and the delta distribution was evaluated. The integration over k_z does only contribute in a prefactor the system we are looking at is two dimensional. The resulting integral in Eq. 11 is a one dimensional integral over the Fermi circle. As can be seen the scattering rate for a magnetic impurity in direction i (Eq. 11) and the i-th component of the spin texture are looking very similar, except that the integral over the Fermi surface adds some level of complexity to it. Despite these small differences, it allows us to to explain a part of the results we find in Tab. I:

The spintexture of the triangular FM case (Fig. 5 right panel) points exclusively in the $+\hat{y}$-direction, thus $s_x = 0$. In this case, introducing a X-impurity will lead to a zero scattering rate or infinite conductivity, whereas a Y-impurity leads to a finite isotropic conductivity. The same is the case for the triangular lattice and the square FM lattice: The spin texture of the triangular lattice pointing along $+\hat{z}$ leading to a suppressed scattering for an X-impurity and a isotropic conductivity for a Z-conductivity. The square FM lattice has a spin texture pointing along $\hat{y}$, leading to divergencies for impurities along $\hat{x}$ and $\hat{z}$.

It is now interesting to compare the triangular FM and the square FM lattice: Both have ferromagnetic moments and a momentum space spin texture pointing in $+\hat{y}$-direction. In both cases, introducing an Y-impurity leads to an isotropic conductivity, hence no AMR. The difference is that the magnetic moments of the square

FM point along $+\hat{y}$, and are thus parallel to the momentum space spin texture, while the magnetic moment of the triangular FM point along $+\hat{z}$ and are thus perpendicular to the momentum space spin texture. Using a Y-impurity projected to sublattice 1 leads to a non-zero AMR (anisotropic conductivity) in case of the triangular FM, but not in case of the square FM, where the conductivity remains isotropic. This can be interpreted in the following way: The projected Y-impurity is only acting on the magnetic moment (pointing along $+\hat{z}$) at sublattice 1 combining impurity and magnetic moment to give the system some degree of collinearity and thus causing AMR. In case of the square FM this is not possible since impurity and magnetic moment are pointing in the same direction. Choosing an impurity poiting elsewhere is also not possible since the momentum spin texture is also pointing along $\hat{y}$, suppressing the contributions from magnetic impurities pointing in other directions.

In case of the non-collinear triangular lattice, the moment space spin texture (not shown, similar to Fig. 5 right panel) points to the $+\hat{z}$ direction. Yet still, a Z-impurity leads to an isotropic conductivity. The reason for this could be that while the impurity is applied in the $\hat{z}$-direction, the conductivity is measured in the xy-plane. There could be a non-zero AMR emerging if we look at the out-of-plane AMR σ_{zz}/σ_{xx} instead. Since we are just looking at a two dimensional model, this would require changes to our model, however.

Now, as a last part of this section, we can look at the crystalline AMR, which refers to the anisotropy of conductivity created by the crystalline symmetry. In our case, this can be defined as:

$$AMR^{cry}_{VW} = \frac{\sigma_{WW}(\hat{M} = \hat{W})}{\sigma_{VV}(\hat{M} = \hat{V})} \tag{12}$$

where V and W are two arbitrary directions (e.g. $\hat{x}$ and $\hat{y}$). The crystalline AMR is thus defind as the quotient as the longitudinal conductivity in V direction for a magnetic impurity in the same direction with the longitudinal conductivity along W for a magnetic impurity in the same direction. In both numerator and denominator are thus longitudinal conductivities with parallel aligned impurity. The resulting anisotropy $AMR^{cry}_{VW} \neq 1$ would thus arise only from the influence of the crystal directions. Calculating the respective quantities for the kagome lattice, we indeed find non-zero crystalline AMR.

V. CONCLUSIONS

Summary and conclusion

- more materials could be investigated, e.g. δ-FeMn or $RbFe(MoO_4)_2$
- All in all, it has to be kept in mind that the model we are using is highly simplistic in its nature. First, the model only contains a hopping and a Heisenberg exchange term. More realistic and complex contributions to systems, such as different atomic orbitals, the crystal field, or the contributions of phonons and magnons, are ignored, as well as any kind of many-body interactions and correlations. For the model systems (thus not in the materials), we also only look into next-neighbor hopping. In the exchange, more complicated (often mid-range) pairings of moments are ignored as well as higher-order contributions such as Dzyaloshinsky-Moriya interaction, which can play a role in such non-collinear systems. It has to be reminded that the spin moments are not just dipole arrows pointing in an direction, but they are spin densities, which contain also higher multipoles
- look at triangular and kagome with e.g. 9 moments in magnetic unit cell.
- propose some experimental method: AMR is traditionally known to be dependent on SOC - it was considered crucial to maximize the SOC to maximize AMR[2]. While SOC cannot be "turned off", we can talk about scaling effects: E.g. finding somewhere (in the classics) how AMR scales with SOC. Then looking at an analogous effect, e.g. AHE and look at Mn_3X (X = Ge[50], Sn[33], Ir[49]), where the atomic number of these 3 is very different → doesnt scale with SOC. Need to find something similar for AMR. Also, ab initio can give rise (compare to[23] - also, there are spin currents in Mn3Sn and -Ge[39]. The discussion is really good there, take some inspiration and refer to it)
- stronger take home message?

ACKNOWLEDGMENTS

Our work benefited from discussions with J. Železný (and Jakub should decide if he wants to be on the author list or not :) and M. Trushin . . . we express our gratitude to them as well as to funding sources from GAČR (under contract 22-21974S).

Appendix A: Ab initio calculations

$\hbar\omega^p_{xx} = 5.87$ eV and $\hbar\omega^p_{zz} = 5.23$ for MnN were obtained using GGA with SO under assumption of 'perfectly cubic lattice constants'; when SO is switched off, we get similar anisotropy...

Appendix B: Further magnetic configuration in the kagome lattice

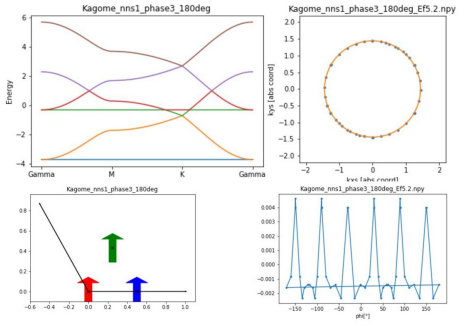

FIG. 6. Results for the kagome lattice, where all moments point towards $+\hat{y}$ (FM state) (left lower panel). Left upper panel: The Bandstructure is still spin-split with two bands being flat (k-independent) on the shown k-range, which can be attibuted to the simplicity of the model. Right upper panel: The Fermi surface (Ef, band?) is represented by the blue dots with the orange circle shown for illustration. The FS is isotropic. Right lower panel: Difference of the FS points the circle. The FS shows a small six-fold modulation on top of an almost perfect spherical symmetry. The system does not show intrinsic AMR.

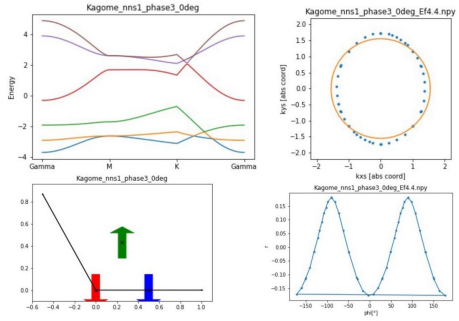

FIG. 7. Collinear ferrimagnetic position. Yes.

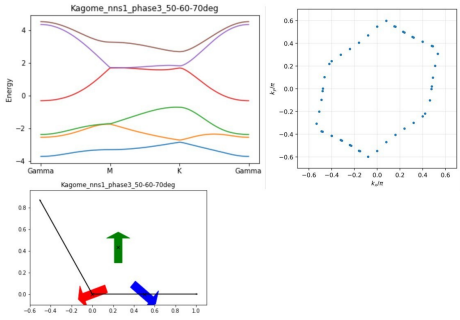

FIG. 8. the famous result

[1] W. Thomson, Proc. R. Soc. Lond. 8, 546.(1857)

[2] P. Ritzinger, K. Výborný, R. Soc. Open Sci., 10, 230564 (2023).

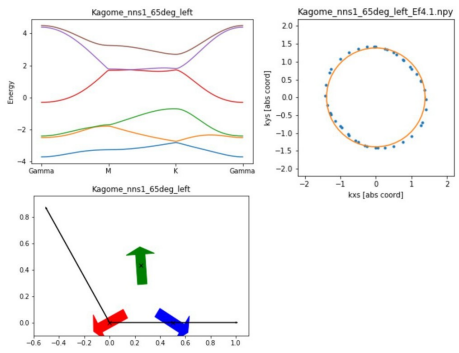

FIG. 9. Simulating magnetic field to the left (-x). Yes

[3] H. S. Alagoz, J. Desomberg, M. Taheri, F. S. Razavi, K. H. Chow, and J. Jung, Appl. Phys. Lett. 106, 082407 (2015)

[4] T. McGuire, T. Potter. IEEE Trans. Magn. 11, 18 (1975)

[5] D. Kriegner, H. Reichlova, J. Grenzer, W. Schmidt, E. Ressouche, J. Godinho, T. Wagner, S. Y. Martin, A. B. Shick, V. V. Volobuev, G. Springholz, V. Holý, J. Wunderlich, T. Jungwirth, and K. Výborný, Phys. Rev. B 96, 214418 (2017).

[6] R. D. Gonzalez Betancourt, J. Zubáč, K. Geishendorf, P. Ritzinger, B. Růžičková, T. Kotte, J. Železný, K. Olejník, G. Springholz, B. Büchner, A. Thomas, K. Výborný, T. Jungwirth, H. Reichlová, and D. Kriegner, npj Spintronics, 2, 45 (2024).

[7] J. Volný, D. Wagenknecht, J. Železný, P. Harcuba, E. Duverger–Nedellec, R. H. Colman, J. Kudrnovský, I. Turek, K. Uhlířrová, K. Výborný, Phys. Rev. Mat. 4, 064403 (2020).

[8] J. Zubáč, Z. Kašpar, F. Krizek, Förster, R. P. Campion, V. Novák, T. Jungwirth, K. Olejník, Phys. Rev. B 104, 184424 (2021).

[9] P. Wadley, B. Howells, J. Železný, C. Andrews, V. Hills, R. P. Campion, V. Novák, K. Olejník, F. Maccherozzi, S. S. Dhesi, S. Y. Martin, T. Wagner, J. Wunderlich, F. Freimuth, Y. Mokrousov, J. Kuneš, J. S. Chauhan, M. J. Grzybowski, A. W. Rushforth, K. W. Edmonds, B. L. Gallagher, T. Jungwirth, Science 351, 6273 (2016).

[10] K. Kabara, M. Tsunoda, S. Kokado, AIP Adv. 7, 056416 (2017).

[11] W. Döring, Ann. Phys. 424, 259-276 (1938).

[12] PRB 79, 045427

[13] P. Ritzinger, H. Reichlová, D. Kriegner, A. Markou, R. Schlitz, M. Lammel, D. Scheffler, G. H. Park, A. Thomas, P. Středa, C. Felser, S. T. B. Goennenwein, and Karel Výborný, Phys. Rev. B, 104, 094406 (2021)

[14] T. Sato, S. Kokado, M. Tsujikawa, T. Ogawa, S. Kosaka, M. Shirai, and M. Tsunoda, Appl. Phys. Express 12, 103005 (2019)

[15] W. Limmer, J. Daeubler, L. Dreher, M. Glunk, W. Schoch, S. Schwaiger, R. Sauer, Phys. Rev. B 77, 205210 (2008).

[16] E. De Ranieri, A. W. Rushforth, K. Výborný, U. Rana, E. Ahmad, R. P. Campion, C, T, Foxon, B. L. Gallagher, A. C. Irvine, J. Wunderlich, New J. Phys. 10, 065003 (2008).

[17] P. Nam Hai, D. Sasaki, L. Duc Anh, M. Tanaka, Appl. Phys. Lett. 100, 262409 (2012). DOI:10.1063/1.4730955

[18] W. Limmer M. Glunk, J. Daeubler, T. Hummel, W. Schoch, R. Sauer, C. Bihler, H. Huebl, M. S. Brandt, S. T. B. Goennenwein, Phys. Rev. B 74, 205205 (2006).

[19] M. Q. Dong, Z.-X. Guo , X. R. Wang, Phys. Rev. B 108, L020401 (2023).

[20] L. Nádvorník, M. Borchert, L. Brandt, R. Schlitz, K. A. de Mare, K. Výborný, I. Mertig, G. Jakob, M. Kläui, S. T.B. Goennenwein, M. Wolf, G. Woltersdorf, T. Kampfrath, Phys. Rev. X 11, 021030 (2021).

[21] J.-H. Park, H.-W. Ko, J.-M. Kim, J. Park, S.-Y. Park, Y. Jo, B.-G. Park, S. K. Kim, K.-J. Lee, K.-J. Kim, Sci. Rep. 11, 20884 (2021).

[22] Bonbien *et al.* J. Phys. D: Appl. Phys. 55, 103002 (2022)

[23] R. González-Hernández, P. Ritzinger, K. Výborný, J. Železný, and A. Manchon, Nat. Commun., 15, 7663 (2024).

[24] S. Granville et al., Phys. Rev. B 72, 205127 (2005).

[25] K. Výborný, J. Kučera, J. Sinova, A. W. Rushforth, B. L. Gallagher, T. Jungwirth, Phys. Rev. B 80, 165204 (2009)

[26] L. M. Corliss, N. Elliot, J. M. Hastings, R. L. Sass, *Phys. Rev.* 122, 1402-1406 (1961).

[27] S. Polesya, S. Mankovsky, D. Benea, H. Ebert, W. Bensch, *J. Phys.: Condens. Matter* 22, 156002 (6pp) (2010).

[28] Y. Tajima, J. Shiogai, K. Ueda, K. Kudo, J. Matsuno, *APL Mater.* 12, 041112 (2024).

[29] C.-Y. Yang, L. Pan, A. J. Grutter, H. Wang, X. Che, Q. L. He, Y. Wu, D. A. Gilbert, P. Shafer, E. Arenholz, H. Wu, G. Yin, P. Deng, J. A. Borchers, W. Ratcliff II, K. L. Wang, *Sci. Adv.* 6, eaaz8463 (2020).

[30] J. Yan, X. Luo, F. C. Chen, Q. L. Pei, G. T. Lin, Y. Y. Han, L. Hu, P. Tong, W. H. Song, X. B. Zhu, Y. P. Sun, *Appl. Phys. Lett.* 111, 022401 (2017).

[31] T. Chen, T. Tomita, S. Minami, M. Fu, T. Koretsune, M. Kitatani, I. Muhammad, D. Nishio-Hamane, R. Ishii, F. Ishii, R. Arita, S. Nakatsuji, *Nat. Commun.* 12, 572 (2021).

[32] K. Manna, Y. Sun, L. Muechler, J. Küebler, C. Felser, "Heusler, Weyl and Berry", *Nat. Rev. Mater.* 3, 244-256 (2018).

[33] S. Nakatsuji, N. Kiyohara, T. Higo, *Nature* 527, 212–215 (2015).

[34] V. Sharma, R. Nepal, R. C. Budhani, *Phys. Rev. B* 108, 144435 (2023).

[35] J. W. Cable, N. Wakabayasi, P. Radhakrishna, *Phys. Rev. B* 48, 6159 (1993).

[36] X. F. Zhou, X. Z. Chen, Y. F. You, L. Y. Liao, H. Bai, R. Q. Zhang, Y. J. Zhou, H. Q. Wu, C. Song, F. Pan, *Phys. Rev. Appl.* 14, 054037 (2020).

[37] M. Ikhlas, T. Tomita, T. Koretsune, M.-T. Suzuki, D. Nishio-Hamane, R. Arita, Y. Otani, S. Nakatsuji, *Nat. Phys.* 13, 1085.

[38] P. Park, J. Oh, K. Uhlířová, J. Jackson, A. Deák, L. Szunyogh, K. H. Lee, H. Cho, H.-L. Kim, H. C. Walker, D. Adroja, V. Sechovský, J.-G. Park, *npj Quantum Materials* 3:63 (2018).

[39] J. Železný, Y. Zhang, C. Felser, B. Yan, *Phys. Rev. Lett.* 119, 187204 (2017).

[40] M. Wu, K. Kondou, T. Chen, S. Nakatsuji, Y. Otani, *AIP Adv.* 13, 045102 (2023).

[41] H. Reichlova, T. Janda, J. Godinho, A. Markou, D. Kriegner, R. Schlitz, J. Zelezny, Z. Soban, M. Bejarano, H. Schultheiss, P. Nemec, T. Jungwirth, C. Felser, J. Wunderlich, S.T.B. Goennenwein, *Nat. Commun.* 10:5459 (2019).

[42] Y. Zhang, Y. Sun, H. Yang, J. Železný, S. P. P. Parkin, C. Felser, B. Yan, *Phys. Rev. B* 95, 075128 (2017).

[43] N. Nagaosa, J. Sinova, S. Onoda, A. H. MacDonald, N. P. Ong, *Rev. Mod. Phys.* 82, 1539 (2010).

[44] I. Bakonyi, F. D. Czeschka, L. F. Kiss, V. A. Isnaini, A. T. Krupp, K. Palotás, S. Zsurzsa, L. Péter, arXiv:2203.11568 [cond-mat.mtrl-sci] (2022).
[45] T. Kato, Y. Ishikawa, H. Itoh, J.-i. Inoue, Phys. Rev. B 77, 233404 (2008).
[46] J. Velev, R. F. Sabirianov, S. S. Jaswal, E. Y. Tsymbal, Phys. Rev. Lett. 94, 127203 (2005).
[47] F. L. Zeng, Z. Y. Ren, Y. Li, J. Y. Zeng, M. W. Jia, J. Miao, A. Hoffmann, W.Zhang, Y. Z. Wu, Z. Yuan, Phys.Rev. Lett. 125, 097201 (2020).
[48] T. Kato, Y. Ishikawa, H. Itoh, J. Inoue, phys. stat. sol. (b) vol. 244, 12, 4403 - 4406 (2007).
[49] H. Iwaki, M. Kimata, T. Ikebuchi, Y. Kobayashi, K. Oda, Y. Shiota, T. Ono, T. Moriyama, Appl. Phys. Lett. 116, 022408 (2020).
[50] N. Kiyohara, T. Tomita, S. Nakatsuji, Phys. Rev. Appl. 5, 064009 (2016). DOI: 10.1103/PhysRevApplied.5.064009
[51] Dunz et al. MnN, DOI: 10.1103/PhysRevResearch.2.013347
[52] `https://www.cryst.ehu.es/magndata/index.php?index=0.199`, 2024-08-23, 12:01
[53] `https://www.cryst.ehu.es/magndata/index.php?this_label=2.35`, 2024-08-14, 15:11
[54] H. Yang *et al*, Phys. Rev. B 104, 214419 (2021).